ORGANIC CHEMISTRY FRONTIERS

CCS 中国化学会 CHINESE CHEMICAL SOCIETY

SIOC

ROYAL SOCIETY OF CHEMISTRY

Dimerization of Indenocorannulene Radicals: Imposing Stability through Increasing Strain and Curvature

Journal:	*Organic Chemistry Frontiers*
Manuscript ID	QO-RES-06-2020-000686.R1
Article Type:	Research Article
Date Submitted by the Author:	08-Jul-2020
Complete List of Authors:	Rogachev, Andrey; Illinois Institute of Technology, Chemistry Zhu, Yikun; University at Albany State University of New York, Chemistry Zhou, Zheng; University at Albany State University of New York, Liu, Shuyang; Illinois Institute of Technology College of Science, Department of Chemistry Wei, Zheng; University at Albany, SUNY, Chemistry Petrukhina, Marina; University at Albany State University of New York, Chemistry

ARTICLE

Dimerization of Indenocorannulene Radicals: Imposing Stability through Increasing Strain and Curvature

Received 00th January 20xx,
Accepted 00th January 20xx

DOI: 10.1039/x0xx00000x

Andrey Yu. Rogachev,*[a] Yikun Zhu,[b] Zheng Zhou,[b] Shuyang Liu,[a] Zheng Wei[b] and Marina A. Petrukhina*[b]

One-electron reduction of bowl-shaped indenocorannulene, $C_{26}H_{12}$, with Rb metal in THF affords $[\{Rb^+(18\text{-crown-6})\}_2(C_{26}H_{12}–C_{26}H_{12})^{2–}]\cdot 4THF$, as confirmed by single-crystal X-ray diffraction. The product consists of a dimeric σ-bonded dianion (C–C, 1.568(7) Å) having two *endo*-η^6 coordinated $\{Rb^+(18\text{-crown-6})\}$ moieties (Rb–C, 3.272(4)–3.561(4) Å). The $(C_{26}H_{12}–C_{26}H_{12})^{2–}$ dimer represents the first crystallographically confirmed example of spontaneous coupling for indenocorannulene monoanion radicals, $C_{26}H_{12}^{\cdot–}$. Comprehensive theoretical investigation of the new dimer confirms the single σ-bond character of the linker and reveals a significant increase of both thermodynamic and kinetic stability of $[\sigma\text{-}(C_{26}H_{12})_2]^{2–}$ in comparison with analogues formed by such π-bowls as corannulene and its dibenzo-derivative. The in-depth computational analysis and direct comparison of the series demonstrates the effect of curvature on radical coupling processes, allowing control over stability and reactivity of bowl-shaped π-radicals.

Introduction

Studies of stability, reactivity, and coupling of planar and curved organic radicals attract significant attention due to fundamental importance[1-4] and potential practical applications.[5,6] Spontaneous dimerization of π-radicals can proceed through two distinctive interaction modes, namely σ- or π-bonding.[7] In addition, examples of fluxional behavior between σ- or π-bonded isomers have been reported.[8-10] Full understanding and control of these processes are important for such diverse areas as mechanistic and synthetic organic chemistry,[11-13] structural and materials chemistry,[14-18] magnetism and conductivity of organic and hybrid solids.[19-21] For non-planar π-radicals, multiple X-ray crystallographic examples of dimeric products formed by the ball-shaped C_{60}-fullerene have been reported to reveal the formation of a single covalent C–C bond connector between two fullerene-cages.[22-26] In contrast, the radical coupling processes of curved polycyclic aromatic hydrocarbons (PAHs), representing fragments of the C_{60}-fullerene,[27-29] have been mainly investigated in solution.[30-32] As revealed spectroscopically, negatively charged bowl-shaped PAHs can undergo complex dimerization and self-assembly processes that are topology and charge-dependent.[30,33] In recent years, this chemistry has been moved from solution to the solid-state to allow X-ray crystallographic characterization of the products. The structures of remarkable sandwich-type supramolecular aggregates have been reported for the highly-negatively charged bowl-shaped corannulene[34-41] with unique coupling pathways observed for corannulene trianions.[39] Upon one-electron addition, corannulene ($C_{20}H_{10}$, **1**) was shown to undergo spontaneous dimerization to afford a dianionic σ-bonded dimer, namely $[\sigma\text{-}(C_{20}H_{10})_2]^{2–}$.[42] A similar dimerization pathway has been also observed for dibenzo[*a*,*g*]corannulene ($C_{28}H_{14}$, **2**).[43] Comprehensive structural and computational investigation of the dimeric products formed by two bowl-shaped radicals of **1** and **2** revealed their thermodynamic instability with respect to decomposition into parent monomeric radicals. However, the high energy barrier for passing through a spin-crossing point during this process allowed the kinetic persistence of both dimers of **1** and **2**. A direct comparison of coupling processes for fullerenes and two shallow bowl-shaped fullerene fragments pointed to the possible effect of curvature on the stability of non-planar π-radicals. As the degree of curvature imposed on bowl-shaped π-systems can be effectively modulated through molecular geometry design,[44-46] π-bowls offer a unique opportunity for systematic investigation of the effects of size, symmetry and strain on radical coupling processes.

In this work, we selected a π-bowl with increased curvature and strain compared to corannulene, namely indenocorannulene ($C_{26}H_{12}$, **3**, Scheme 1). We investigated the rubidium-induced chemical reduction of **3** in THF and successfully isolated the product of one-electron reduction step. The first product based on the coupling of two $\mathbf{3}^{\cdot–}$ radicals has been crystallographically and spectroscopically characterized, followed by a comprehensive theoretical analysis of its electronic structure, thermodynamic and kinetic stability.

[a]*Department of Chemistry, Illinois Institute of Technology, Chicago, IL 60616, USA E-mail: arogache@iit.edu*
[b]*Department of Chemistry, University at Albany, State University of New York, Albany, NY 12222, USA. E-mail: mpetrukhina@albany.edu*
Electronic Supplementary Information (ESI) available: Synthetic procedures, X-ray crystallographic details, UV-vis and NMR spectroscopic data, Computational details. CCDC 2007818. For ESI and crystallographic data in CIF or other electronic format see DOI: 10.1039/x0xx00000x

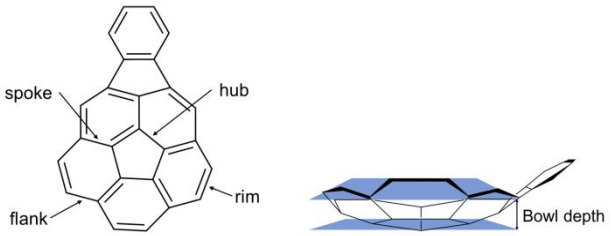

Scheme 1 Depiction of indenocorannulene (**3**) along with the bowl depth calculation.

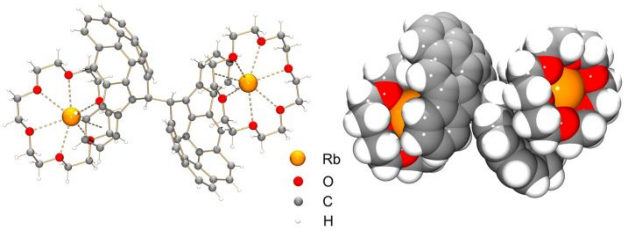

Fig. 1 Crystal structure of **4**, ball-and-stick and space-filling models.

Results and discussion

Chemical reduction of 3

The synthesis of indenocorannulene, $C_{26}H_{12}$ (**3**), has been reported back in 2001.[47] The X-ray crystal structural characterization of **3** has confirmed its increased bowl depth of 1.065(4) Å[45,46] *vs.* that of corannulene (0.875(2) Å).[48] Chemical reduction of **3** has been first investigated by Scott and Rabinovitz in solution, using a combination of spectroscopic methods.[30] These studies demonstrated very rich redox chemistry of **3** coupled with complex dimerization and supramolecular aggregation processes that the negatively-charged indenocorannulene can undergo in solution. The only prior example of metal complexation for **3** has revealed an increasing bowl curvature from direct metal binding.[49] Despite these intriguing observations, no crystallographically confirmed examples stemming from the electron-transfer processes of **3** have been reported to date.

In this work, the chemical reduction of **3** has been carried out with rubidium metal in THF at room temperature. Short reaction time (*ca*. 1 h) and the addition of 18-crown-6 ether have been used to facilitate crystallization of the monoreduced state of **3**. Slow diffusion of hexanes into a reaction solution allowed the isolation of brown crystals of good quality.

Crystallographic characterization of 4

The X-ray diffraction characterization of the above crystals (See the Supporting Information for more details) revealed the formation of $[\{Rb^+(18\text{-crown-6})\}_2(C_{26}H_{12}–C_{26}H_{12})^{2–}]$ (**4**), crystallized with four THF molecules as **4**·4THF.

In the crystal structure of **4**, the dimeric dianion is centrosymmetric with only a half of its core being crystallographically independent (Fig. S10). Two cationic $\{Rb^+(18\text{-crown-6})\}$ moieties coordinate to the concave surfaces of the dimer (Fig. 1), with four interstitial THF molecules filling the voids (Fig. S11). Specifically, the Rb^+ ions bind to the six-membered ring of the indenyl group in an asymmetric *endo*-η^6-fashion, with the Rb···C distances spanning over 3.272(4)–3.561(4) Å (Fig. S12). The coordination environment of each Rb^+ ion is completed by an axially bound 18-crown-6 ether (Rb···O, 2.832(2)–2.980(3) Å). All Rb···C and Rb···O distances are comparable to those reported previously.[50-55] Some additional intramolecular C–H···π contacts are found between the 18-crown-6 ether and the concave bowl cavity of the dimeric dianion, spanning a broad range of 2.598–3.053 Å. In the solid state structure of **4** (Fig. S13), intermolecular C–H···π interactions (2.560(5)–2.722(5) Å) between the convex bowl faces of the dianions and the adjacent 18-crown-6 ether moieties are responsible for the formation of a 2D layer. No significant interactions are found between the adjacent layers.

In the centrosymmetric $(C_{26}H_{12}–C_{26}H_{12})^{2–}$ dimer, the C–C bond length of the linker at 1.556(5) Å and average bond angle of 109.5(3)° are indicative of the formation of a single C–C bond and the sp^3-hybridization of the C16 atom at the connecting site (Table 1). In comparison to the neutral parent, the hub (1.410(5)–1.433(5) Å) and rim (1.375(6)–1.545(5) Å) C–C bonds of the mono-reduced indenocorannulene bowl in **4** are slightly elongated. In contrast, the C–C bonds of the indenyl group are slightly shortened (1.371(5)–1.450(5) Å in **4** *vs.* 1.383(4)–1.498(4) Å in **3**, Table 2). Interestingly, the depth of the corannulene bowl (1.029(5) Å) in the dimer in **4** is slightly reduced compared to that in the neutral indenocorannulene (1.065(4) Å).[45]

Following the bowl depth alteration, the POAV calculations were also used to describe the change of pyramidalization for each C-atom upon one-electron acquisition and dimerization processes (Tables 3, S2). In the neutral bowl, the highest value

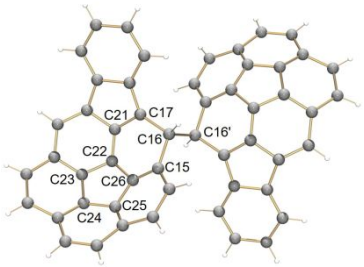

Table 1 Selected C–C bond length distances (Å) and angles (°) in $C_{26}H_{12}$ (**3**) and the dimer in **4** along with a labelling scheme.

		$C_{26}H_{12}$[45]	$[\sigma\text{-}(C_{26}H_{12})_2]^{2–}$
Bond Distance	C16–C16′	–	1.568(7)
	C15–C16	1.460(4)	1.554(5)
	C16–C17	1.385(4)	1.545(5)
Bond Angle	C15–C16–C16′	–	109.5(3)
	C15–C16–C17	120.3(4)	109.4(3)
	C16′–C16–C17	–	112.9(4)

of POAV angle was found at C22 (11.42°) of the central five-membered ring. Notably, the POAV value of C22 has increased to 13.24° in the dianionic dimer. However, the most pyramidalized carbon site in the $(C_{26}H_{12}–C_{26}H_{12})^{2–}$ dimer is the sp^3-hybridized C16-atom, with a POAV angle of 18.31°. Except for C16 and C22, the remaining C-atoms become less pyramidalized in **4** than those in the neutral parent, which is consistent with the observed decrease of the bowl depth in the dimer.

A similar dimerization pathway has been recently observed for the monoreduced corannulene $(C_{20}H_{10})$[42] and dibenzo[*a*,*g*]corannulene $(C_{28}H_{14})$[43] affording the products of the corresponding dianionic dimers in the solid state. The C–C bond length of the linker and bond angles at the connecting site in **4** are close to those in the $[\sigma\text{-}(C_{20}H_{10})_2]^{2–}$ and $[\sigma\text{-}(C_{28}H_{14})_2]^{2–}$ dimers (Tables 4, S3).

Although geometric parameters of the dimeric products show close match, the solution behavior is different. Both the $[\sigma\text{-}(C_{20}H_{10})_2]^{2–}$ and $[\sigma\text{-}(C_{28}H_{14})_2]^{2–}$ dimers were found to fall apart in solution.[42,43] In contrast, the ^{1}H NMR spectroscopic data of **4** demonstrate the persistence of the new dimer in solution at room temperature (Figs. S3, S4), and even upon heating (Fig. S7). Specifically, the proton (H16) bound to the sp^3 hybridized C16 atom is largely shielded with the signal shifted to 5.75 ppm compared to that in neutral **3** (7.74 ppm, Fig. S5). Except for the protons on C2 and C5 atoms (See Table S2 for numbering), the remaining ^{1}H NMR signals of $[\sigma\text{-}(C_{26}H_{12})_2]^{2–}$ are up-field shifted, stemming from the charge distribution rearrangement during reduction and dimerization. Notably, the NMR data for the dissolved crystals of **4** are consistent with the previous *in situ* NMR solution study of the K-induced indenocorannulene reduction.[30] Moreover, the ^{1}H NMR signal shifts calculated in this work (Fig. S18) show close match with experimental values. Finally, it should be pointed out that the $(C_{26}H_{12}–C_{26}H_{12})^{2–}$ dimer can dissociate and re-oxidize back to neutral **3**, as confirmed by ^{1}H NMR upon quenching with air (Fig. S8).

Table 4 Key distances (Å) and angles (°) for the series of dimers.

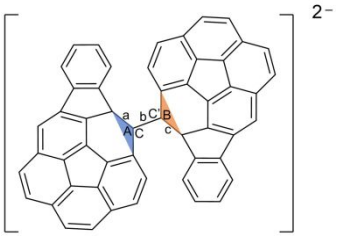

	$[\sigma\text{-}(C_{20}H_{10})_2]^{2–}$	$[\sigma\text{-}(C_{28}H_{14})_2]^{2–}$	$[\sigma\text{-}(C_{26}H_{12})_2]^{2–}$
C–C′ distances	1.588(5)	1.559(8)	1.568(7)
Average bond angle	111.1(1)	110.4(1)	109.5(3)
Bowl depth	0.906(5)	0.891(9)	1.029(5)
Torsion angle a–b–c	180(1)	172.91(1)	180(3)
Dihedral angle ∠A/B	0(1)	4.98(1)	0(3)

Another confirmation of existence of the dimeric species in solution comes from UV-Vis spectroscopic study of target systems. The nature of characteristic transition at 764 nm (Fig. S2) was further clarified through theoretical TD-DFT calculations (see ESI for more details), which exhibited an excellent agreement (761 nm, Fig. S19) with the above experimental value. This band is described by a HOMO-LUMO transition (Fig. S21). The HOMO corresponds to the σ-bonding between two bowl-shaped fragments, whereas the LUMO is a purely delocalized π-orbital of the polyaromatic unit. Expectedly, such transition is absent in both calculated and experimental UV-Vis spectra of the neutral indenocorannulene. Moreover, the same transition computed for an isolated dianionic dimer (without directly interacting with Rb^+ cations) showed a significant shift to 799 nm. Thus, UV-Vis spectroscopy not only provides a clear evidence of existence of the dimeric species in solution, but also points out to the formation of contact-ion pars rather than solvent-separated ones.

For the next step, in order to quantify the stability and energetics of the new dimeric product, we turned to its comprehensive theoretical investigation.

Theoretical analysis

Indenocorannulene monoanion radical, $C_{26}H_{12}^{\cdot-}$. Prior to theoretical description of the new dimer, we have analyzed the parent monoanion, $C_{26}H_{12}^{\cdot-}$, with a special focus on how the alkali metal coordination (with and without extra ligand) influences the geometry and electronic structure of this bowl-shaped radical. The optimized geometries and 3D spin density distribution of $C_{26}H_{12}^{\cdot-}$ are shown in Fig. 2.

An addition of one electron to indenocorannulene results in a small but notable decrease of the bowl depth from 1.077 Å in neutral parent to 1.046 Å in the monoreduced state of **3**. This is in perfect agreement with the previously reported trend of flattening of bowl-shaped polyarenes upon addition of electrons.[56] Interestingly, complexation of the $C_{26}H_{12}^{\cdot-}$ ligand with Rb^+ to form a contact-ion pair (CIP) is accompanied by an increase of the bowl depth of $C_{26}H_{12}^{\cdot-}$ to 1.084 Å. However, a subsequent addition of a strong donor, 18-crown-6 ether (18C6), to the coordination environment of Rb^+ reverses the

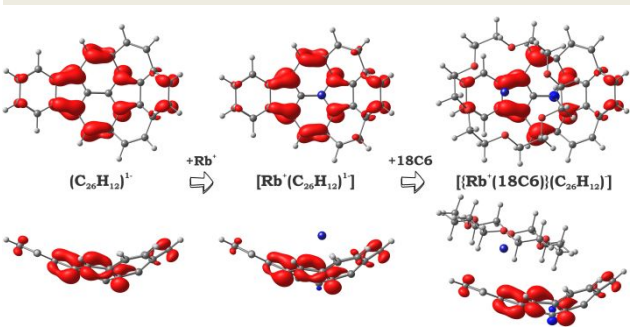

Fig. 2 Spin density distribution (isosurface 0,0035 a.u.) in indenocorannulene radical-based systems (PBE0/cc-pVTZ(C,H,O)//def2-TZVP(Cs)).

Table 2 Key C–C bond length distances and bowl depth (Å) in $C_{26}H_{12}$ and $[\sigma\text{-}(C_{26}H_{12})_2]^{2-}$.

	$C_{26}H_{12}$[45]	$[\sigma\text{-}(C_{26}H_{12})_2]^{2-}$
Hub	1.404(4)–1.424(4)	1.410(5)–1.433(5)
Rim	1.372(4)–1.385(4)	1.375(5)–1.545(5)
Spoke	1.356(4)–1.397(4)	1.370(5)–1.399(5)
Flank	1.429(3)–1.460(3)	1.390(5)–1.554(5)
Indenyl group	1.383(4)–1.498(4)	1.371(5)–1.450(5)
Bowl depth	1.065(4)	1.029(5)

Table 3 Selected average p-orbital axis vector (POAV) angles (°) in $C_{26}H_{12}$ and $[\sigma\text{-}(C_{26}H_{12})_2]^{2-}$.

POAV	$C_{26}H_{12}$[45]	$[\sigma\text{-}(C_{26}H_{12})_2]^{2-}$	Δ
C15	4.70	2.29	–2.41
C16	3.44	18.31	14.87
C17	4.97	3.51	–1.46
C21	6.68	6.54	–0.14
C22	11.15	13.24	2.09
C23	9.82	9.34	–0.48

trend back to a reduced bowl depth (1.021 Å), which agrees well with the experimental value (Table 2). The detected difference between the complexes of $C_{26}H_{12}^{\cdot-}$ with the naked Rb^+ and complexed {Rb^+(18C6)} cations can be attributed to significant changes in their geometries, as illustrated in Fig. 2. While in $[Rb^+(C_{26}H_{12}^{\cdot-})]$, a symmetrical metal ion placement inside the bowl is observed, the $[\{Rb^+(18C6)\}(C_{26}H_{12}^{\cdot-})]$ complex shows a clear shift in binding towards the indeno-site of the ligand (Fig. 2). This could be indicative of a strong network of C–H···π interactions between the crown ether and the negatively charged $C_{26}H_{12}^{\cdot-}$ anion, which stabilizes a specific geometrical configuration. Indeed, multiple C–H···π interactions have been detected in the X-ray crystal structure of **4**.

Despite the difference observed in geometry of $[Rb^+(C_{26}H_{12}^{\cdot-})]$ and $[\{Rb^+(18C6)\}(C_{26}H_{12}^{\cdot-})]$, the localization of unpaired electron was found to be exactly the same for both, as evidenced by spin density distribution (Fig. 2). Such a minimal influence of the counter ion (with and without a spectator ligand) on spin density distribution over the polyaromatic core has been observed earlier.[57] Compared to the highly symmetric $C_{20}H_{10}^{\cdot-}$ bowl,[42] fusion of the indeno-group to the corannulene

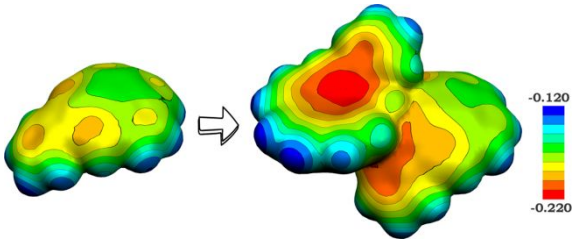

Fig. 3 Redistribution of negative charge over π-surface during radical coupling, as illustrated by MEP maps of $C_{26}H_{12}^{\cdot-}$ (*left*) and $[\sigma\text{-}(C_{26}H_{12})_2]^{2-}$ (*right*) (PBE0/cc-pVTZ).

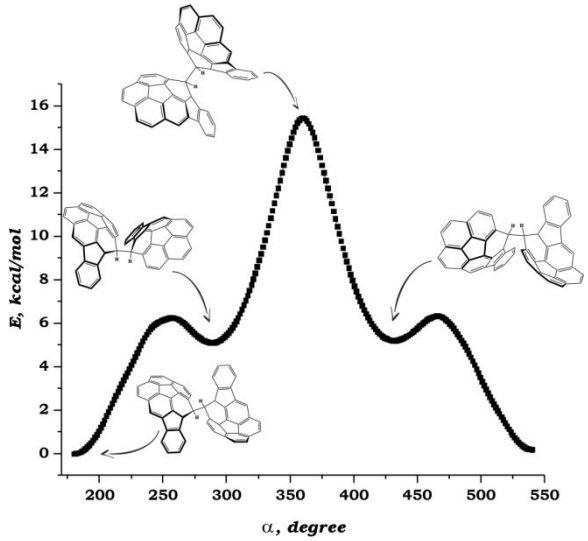

Fig. 4 Potential energy profile for the rotation of indenocorannulene fragments in $[\sigma\text{-}(C_{26}H_{12})_2]^{2-}$ around the C–C′ linker (PBE0/cc-pVTZ).

core causes a significant redistribution of the spin density in $C_{26}H_{12}^{\cdot-}$ with its notable localization at the junction between the two fused parts. Specifically, the highest spin value is found at the rim site adjacent to the junction. This observation unambiguously explains the subsequent dimerization process, which occurs exclusively at this specific C-atom with the highest spin population, as confirmed crystallographically in **4**. This also supports the idea of an artificially created spin center (carbon atom carrying the largest spin) that was successfully utilized in the design of the first dianionic dimer using dibenzo[*a,g*]corannulene.[43] The formation of a new site-directed σ-bonded dimer formed by indenocorannulene monoanion radicals further reinforces this designed concept.

Electronic structure of the dimer. In order to further support the hypothesis of the direct correlation between the spin density localization and energetic preference for a given isomer, we have tested all possible σ-bonded dimers formed by $C_{26}H_{12}^{\cdot-}$ radicals with different C–C coupling sites (Fig. S14). Surprisingly, only two dimeric systems were found to correspond to local minima in the potential energy surface (Fig. S15). The rest diverged during optimization procedure or eventually converged to one of these two dimers. The most energetically favorable dianionic dimer (by +48.59 kcal/mol) strictly corresponds to the configuration observed experimentally.

Similar to the $[\sigma\text{-}(C_{20}H_{10})_2]^{2-}$ and $[\sigma\text{-}(C_{28}H_{14})_2]^{2-}$ products,[42,43] the ground state of the title dimer having the lowest energy was found to be a closed-shell singlet. The latter is energetically well-isolated from the triplet and open-shell singlet states (by >20 kcal/mol). Analysis of the bonding between the bowl-shaped fragments revealed that the C–C′ linker is best described as a single non-polar covalent bond of σ-type, which is supported by both geometrical parameters and NBO analysis (Fig. S16). Interestingly, an addition of the rubidium counterion (with or without crown ether) shows almost negligible impact on the nature of this C–C′ bond. A 3D distribution of negative

Table 5 Results of EDA analysis for $[\sigma\text{-}(C_{26}H_{12})_2]^{2-}$, $[\{Rb^+\}_2\{\sigma\text{-}(C_{26}H_{12})^{2-}\}]$, and $[\{Rb^+(18C6)\}_2\{\sigma\text{-}(C_{26}H_{12})^{2-}\}]$ systems (PBE0/TZ2P/ZORA; kcal/mol).

Parameter	$[\sigma\text{-}(C_{20}H_{10})_2^{2-}]$[42]	$[\sigma\text{-}(C_{28}H_{14})_2^{2-}]$[42]	$[\sigma\text{-}(C_{26}H_{12})_2^{2-}]$	$[\{Rb^+\}_2\{\sigma\text{-}(C_{26}H_{12})^{2-}\}]$	$[\{Rb^+(18C6)\}_2\{\sigma\text{-}(C_{26}H_{12})^{2-}\}]$
ΔE_{int}	-21.72	-28.52	-34.66	-85.35	-82.56
ΔE_{orb}	-324.54	-320.24	-345.89	-341.37	-339.83
ΔE_{elstat}	-142.60	-141.14	-141.70	-180.14	-185.18
ΔE_{Pauli}	+445.42	+432.86	+452.94	+436.16	+442.45
ΔE_{prep}	+59.98	+64.05	+66.16	+69.15	+66.63
$-D_e$	+38.26	+35.53	+31.50	-16.20	-15.93

charge over the indenocorannulene surface upon formation of the $[\sigma\text{-}(C_{26}H_{12})_2]^{2-}$ dimer (Fig. 3) corresponds to localization of the previously unpaired and delocalized electrons at the C–C′ bonding site. Subsequent evaluation of the conformational stability of the $[\sigma\text{-}(C_{26}H_{12})_2]^{2-}$ system clearly indicates the highest stability of the *trans*-conformer by at least ~6 kcal/mol, as compared with two other isomers (Fig. 4). Such stabilization can be explained by minimization of the electrostatic repulsion between two negatively charged indenocorannulene bowls of the dianionic dimer. Importantly, the *trans*-conformer has been observed in the X-ray crystal structure of **4**. All these findings are in excellent agreement with two analogous members of this series.[42,43]

Energetics of dimerization. For the next step, evaluation of the energetics of decomposition of the closed-shell singlet dimer $[\sigma\text{-}(C_{26}H_{12})_2]^{2-}$ (S = 0) into two radicals $C_{26}H_{12}^{\cdot-}$ with the total spin of S = 1 (S = 1/2 for each monoanion) has been completed. Previously, the dimers were found to be thermodynamically unstable (having $-D_e$ or $E_{bonding}$ positive in magnitude) but kinetically persistent due to a spin-crossing point at the intersection of two potential energy surfaces, namely the singlet and triplet ones.[42,43]

Indeed, the calculated bonding energy for the new dimer was also found to be positive (+31.50 kcal/mol). However, when compared with the same parameter computed for corannulene and dibenzo[*a,g*]corannulene derivatives, the $[\sigma\text{-}(C_{26}H_{12})_2]^{2-}$ dimer clearly shows the highest stability (by *ca*. 6 kcal/mol) mainly due to substantial increase of the total interaction energy (ΔE_{int} of −34.66 kcal/mol *vs*. −21.72 kcal/mol for $[\sigma\text{-}(C_{20}H_{10})_2]^{2-}$ and −28.52 kcal/mol for $[\sigma\text{-}(C_{28}H_{14})_2]^{2-}$ calculated at the same level of theory[42]). Subsequent detalization of contributions from different attractive (covalent or ΔE_{orb} and ionic ΔE_{elstat}) and repulsive (ΔE_{Pauli}) components of bonding clarified the observed trend. Whereas the ΔE_{elstat} remains essentially the same (within Δ = 2 kcal/mol) for all members of the series, the orbital term was found to be ~25 kcal/mol larger in the indenocorannulene derivative. It should be noted here that non-planarity of polyaromatic surface leads to asymmetric shape of π-orbitals with greater localization on the *exo*-side. This results in notable localization of electron density on the convex surface and, consequently, to more efficient convex-convex orbital overlap when interacting with another reactive species. Thus, the larger ΔE_{orb} in the title system as compared with corannulene and dibenzo[*a,g*]corannulene derivatives can be stemming from the higher curvature of the π-surface of bowl-shaped fragments in $[\sigma\text{-}(C_{26}H_{12})_2]^{2-}$ (Table 5). Usually, larger orbital component is accompanied by greater Pauli repulsion. Indeed, for the indenocorannulene dimer ΔE_{Pauli} was calculated to be the largest among three dimeric analogues (Table 5).

Influence of the counterion. Complexation of the dianionic dimer $[\sigma\text{-}(C_{26}H_{12})_2]^{2-}$ with two rubidium cations results in a dramatic change of the thermodynamic stability of the system (Table 5). Whereas the parent "naked" dimer is thermodynamically unstable, the complexed one shows remarkable stability as evaluated by bonding energy ($-D_e$). As follows from different contributions to the total bonding, the key player in reversing the stability is the electrostatic component of the ionic term, which increases substantially (by ~40 kcal/mol) from "naked" $[\sigma\text{-}(C_{26}H_{12})_2]^{2-}$ dimer to its complex, $[\{Rb^+\}_2\{\sigma\text{-}(C_{26}H_{12})^{2-}\}]$ (Table 5). At the same time, the covalent component goes slightly down (by ~4 kcal/mol) in that direction. In spite of the fact that the addition of the spectator 18-crown-6 ether led to changing the Rb^+ binding site (Fig. 2),

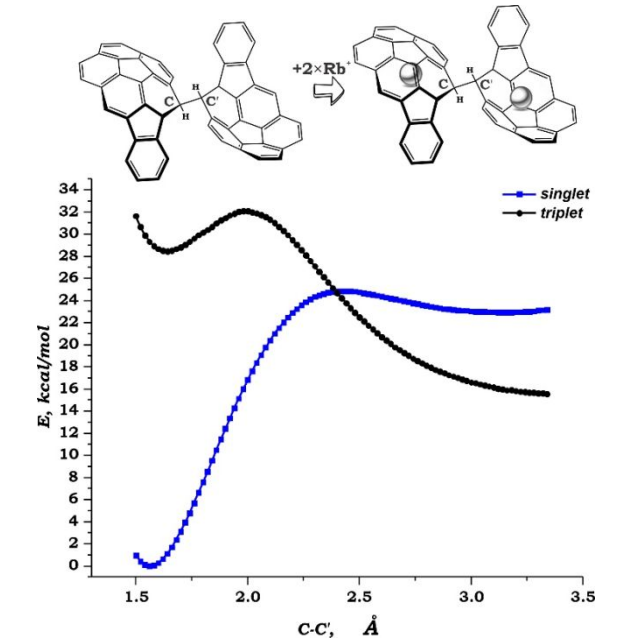

Fig. 5 Stabilization of the $[\sigma\text{-}(C_{26}H_{12})_2]^{2-}$ dimer by Rb^+ counterions, as evidenced by PET scan for the C–C′ connecting bond breaking/forming process for different spin-states (PBE0/TZVP/ZORA).

its influence on thermodynamic stability of the resulting product was found to be small ($-D_e$ varies within 0.5 kcal/mol).

Importantly, when compared with two previously reported analogues, the indenocorannulene derivative is *incredibly stable* with $-D_e$ calculated to be almost twice larger in magnitude (−16.20 kcal/mol *vs*. −9.27 and −9.97 kcal/mol for $[\sigma\text{-}(C_{20}H_{10})_2]^{2-}$ and $[\sigma\text{-}(C_{28}H_{14})_2]^{2-}$ dimers[57]). As in the case of "naked" dianions, the orbital component of the bonding plays the key role in such stabilization, being significantly (by ~25 kcal/mol) greater than those calculated for the $[\{Cs^+\}_2\{\sigma\text{-}(C_{20}H_{10})^{2-}\}]$ and $[\{Cs^+\}_2\{\sigma\text{-}(C_{28}H_{14})^{2-}\}]$ adducts. Thus, one can conclude that the increase of the curvature of the π-bowl-shaped radicals dramatically rises the thermodynamic stability of the resulting dimeric σ-bonded products. This effect is even more pronounced when coupled with complexation of the dianions with alkali metal cations.

Kinetic stability. We have previously observed that the thermodynamically unstable $[\sigma\text{-}(C_{20}H_{10})_2]^{2-}$ and $[\sigma\text{-}(C_{28}H_{14})_2]^{2-}$ dimers show notable kinetic persistence. The latter is mainly caused by the spin-crossing point between the closed-shell singlet and triplet potential energy surfaces, which the system passing during the decomposition reaction. In this process, a dianionic species $[(PAH)_2^{2-}]$ (S = 0) dissociates into two monoanion-radicals $[(PAH)^{\cdot-}]$ with a total spin of S = 2/2. Together with aforementioned thermodynamic considerations, it completes the picture of the total stability of the target systems.

In order to evaluate the kinetic barrier, the C–C′ connecting bond scan was performed for both potential energy surfaces, closed-shell singlet and triplet. The scan was completed for the C–C′ bond length distances ranging from 1.50 Å to 3.50 Å with a step of 0.02 Å for both $[\sigma\text{-}(C_{26}H_{12})_2]^{2-}$ and $[\{Rb^+\}_2\{\sigma\text{-}(C_{26}H_{12})_2\}^{2-}]$. The energy barrier evaluated as the crossing point between the singlet and triplet surfaces was calculated to be +20.70 kcal/mol and +24.79 kcal/mol, respectively. It is worth to mention that the increase of curvature of the bowl-shaped fragments led to substantial rise of the kinetic barrier in the title dimer as compared with $[\sigma\text{-}(C_{20}H_{10})_2]^{2-}$ and $[\sigma\text{-}(C_{28}H_{14})_2]^{2-}$ (+10.00 kcal/mol and +12.35 kcal/mol, respectively).[42,43] Moreover, subsequent complexation of the $[\sigma\text{-}(C_{26}H_{12})_2]^{2-}$ dimer resulted in enhanced stabilization, making the indenocorannulene derivative the most stable dimeric product known to date for bowl-shaped radicals. For comparison, the calculated barriers are +15.85 kcal/mol and +18.50 kcal/mol for $[\{Cs^+\}_2\{\sigma\text{-}(C_{20}H_{10})^{2-}\}]$ and $[\{Cs^+\}_2\{\sigma\text{-}(C_{28}H_{14})^{2-}\}]$, respectively.[57] An increase of both the thermodynamic and kinetic stability of the new dimer is illustrated in Fig. 5.

Conclusions

In this work, the first crystallographically confirmed example of spontaneous coupling for indenocorannulene monoanion radicals to afford the new $[\sigma\text{-}(C_{26}H_{12})_2]^{2-}$ dimer is reported. The C–C bond formation (1.568(7) Å) is observed at the rim sites of $C_{26}H_{12}^{\cdot-}$ having the highest spin density. This coupling is accompanied by the change of the C-atoms of the linker to sp^3-hybridization (avg. 110.6°). Notably, ^{1}H NMR spectroscopic data for the $[\sigma\text{-}(C_{26}H_{12})_2]^{2-}$ dimer indicate a re-aromatization of these C-atoms as well as an increased stability and persistence of the σ-bonded dimer in solution. The latter was further supported by UV-Vis spectroscopy accompanied by the detailed TD-DFT calculations. This behavior contrasts that for the dimers formed by shallow corannulene and dibenzo[*a,g*]corannulene radicals that dissociate in solution. Moreover, in-depth theoretical analysis of the $[\sigma\text{-}(C_{26}H_{12})_2]^{2-}$ dimer showed it to be the most thermodynamically and kinetically stable product among the analogues formed by bowl-shaped radicals that are known to date (Table 5). Investigation of the bonding between the bowl-shaped fragments identified a dramatically increased orbital/covalent contribution (by ~20 kcal/mol) as a key contributor to the total stability of the $[\sigma\text{-}(C_{26}H_{12})_2]^{2-}$ dimer, when compared with more shallow corannulene or dibenzo[*a,g*]corannulene derivatives. Subsequent complexation of the dianionic dimer by two Rb^+ counterions (with or without spectator 18-crown-6 ether ligand) led to the formation of thermodynamically stable adducts as revealed by the total bonding energy calculations. Notably, the kinetic stability, calculated as the singlet-triplet spin-crossing point, was found to be almost twice larger in the magnitude in the case of indenocorannulene derivatives than in any other dimer formed by bowl-shaped π-radicals. Altogether, these findings clearly reveal the effect of curvature on radical coupling processes and the product energetics, allowing the modulation of stability of the resulting dimers through imposed curvature and strain of monomeric building units.

Conflicts of interest

There are no conflicts to declare.

Acknowledgements

Financial and instrumentational support of this work from the U.S. National Science Foundation (CHE-1608628, CHE-2003411, and MRI-1726724) is gratefully acknowledged (M. A. P.). Financial support from Illinois Institute of Technology (A. Yu. R) and partial support from the Wanger Institute for Sustainable Energy Research (WISER) Seed Grant (A. Yu. R) are also appreciated.

Notes and references

1 R. G. Hicks, *Stable radicals: fundamentals and applied aspects of odd electron compounds*, Wiley, Chichester, 2010.
2 M. Mas-Torrent, N. Crivillers, C. Rovira and J. Veciana, Attaching persistent organic free radicals to surfaces: how and why, *Chem. Rev.*, 2012, **112**, 2506-2527.
3 M. D. Tzirakis and M. Orfanopoulos, Radical reactions of fullerenes: from synthetic organic chemistry to materials science and biology, *Chem. Rev.*, 2013, **113**, 5262-5321.
4 M. B. Casu, Nanoscale studies of organic radicals: surface, interface, and spinterface, *Acc. Chem. Res.*, 2018, **51**, 753-760.
5 I. Ratera and J. Veciana, Playing with organic radicals as building blocks for functional molecular materials, *Chem. Soc. Rev.*, 2012, **41**, 303-349.

6 M. Fourmigué, *The importance of pi-interactions in crystal engineering: frontiers in crystal engineering*, Wiley, Chichester, 2012.
7 Z. Mou, K. Uchida, T. Kubo and M. Kertesz, Evidence of *σ*- and *π*-dimerization in a series of phenalenyls, *J. Am. Chem. Soc.*, 2014, **136**, 18009-18022.
8 D. Small, S. V. Rosokha, J. K. Kochi and M. Heard-Gordon, Intermolecular *π*-to-*π* bonding between stacked aromatic dyads. Experimental and theoretical binding energies and near-IR optical transitions for phenalenyl radical/radical versus radical/cation dimerizations, *J. Phys. Chem*. A 2005, **109**, 11261-11267.
9 H. Phan, K. Lekin, S. M. Winter, R. T. Oakley and M. Shatruk, Photoinduced solid state conversion of a radical *σ*-dimer to a *π*-radical pair, *J. Am. Chem. Soc.*, 2013, **135**, 15674-15677.
10 K. Uchida, Z. Mou, M. Kertesz and T. Kubo, Fluxional *σ*-bonds of the 2,5,8-trimethylphenalenyl dimer: direct observation of the sixfold *σ*-bond shift via a *π*-dimer, *J. Am. Chem. Soc.*, 2016, **138**, 4665-4672.
11 K. Imato, M. Nishihara, T. Kanehara, Y. Amamoto, A. Takahara and H. Otsuka, Self-healing of chemical gels cross-linked by diarylbibenzofuranone-based trigger-free dynamic covalent bonds at room temperature, *Angew. Chem. Int. Ed.*, 2012, **51**, 1138-1142.
12 K. Uchida, S. Ito, M. Nakano, M. Abe and T. Kubo, Biphenalenylidene: isolation and characterization of the reactive intermediate on the decomposition pathway of phenalenyl radical, *J. Am. Chem. Soc.*, 2016, **138**, 2399-2410.
13 K. Kato and A. Osuka, Platforms for stable carbon-centered radicals, *Angew. Chem. Int. Ed.*, 2019, **58**, 8978-8986.
14 X. Chen, X. Wang, Z. Zhou, Y. Li, Y. Sui, J. Ma, X. Wang and P. P. Power, Reversible *σ*-dimerizations of persistent organic radical cations, *Angew. Chem. Int. Ed.*, 2013, **52**, 589-592.
15 J. L. Zafra, L. Qiu, N. Yanai, T. Mori, M. Nakano, M. P. Alvarez, J. T. Navarrete, C. J. Gomez-Garcia, M. Kertesz, K. Takimiya and J. Casado, Reversible dimerization and polymerization of a janus diradical to produce labile C-C bonds and large chromic effects, *Angew. Chem. Int. Ed.*, 2016, **55**, 14563-14568.
16 H. Yokoi, S. Hiroto and H. Shinokubo, Reversible *σ*-bond formation in bowl-shaped *π*-radical cations: the effects of curved and planar structures, *J. Am. Chem. Soc.*, 2018, **140**, 4649-4655.
17 K. Okino, D. Sakamaki and S. Seki, Dicyanomethyl radical-based near-infrared thermochromic dyes with high transparency in the visible region, *ACS Mater. Lett.*, 2019, **1**, 25-29.
18 L. Moshniaha, M. Żyła-Karwowska, P. J. Chmielewski, T. Lis, J. Cybińska, E. Gońka, J. Oschwald, T. Drewello, S. M. Rivero, J. Casado and M. Stępień, Aromatic nanosandwich obtained by *σ*-dimerization of a nanographenoid *π*-radical, *J. Am. Chem. Soc.*, 2020, **142**, 3626-3635.
19 J. L. Segura and N. Martín, [60]Fullerene Dimers, *Chem. Soc. Rev.*, 2000, **29**, 13-25.
20 D. V. Konarev, S. S. Khasanov and R. N. Lyubovskaya, Fullerene complexes with coordination assemblies of metalloporphyrins and metal phthalocyanines, *Coord. Chem. Rev.*, 2014, **262**, 16-36.
21 A. Dragulescu-Andrasi, A. S. Filatov, R. T. Oakley, X. Li, K. Lekin, A. Huq, C. Pak, S. M. Greer, J. McKay, M. Jo, J. Lengyel, I. Hung, E. Maradzike, A. E. DePrince, S. A. Stoian, S. Hill, Y.-Y. Hu and M. Shatruk, Radical dimerization in a plastic organic crystal leads to structural and magnetic bistability with wide thermal hysteresis, *J. Am. Chem. Soc.*, 2019, **141**, 17989-17994.
22 J. R. Morton, K. F. Preston, P. J. Krusic, S. A. Hill and E. Wasserman, The dimerization of fullerene RC_{60} radicals [R = alkyl], *J. Am. Chem. Soc.*, 1992, **114**, 5454-5455.
23 K. Komatsu, K. Fujiwara, T. Tanaka and Y. Murata, The fullerene dimer C_{120} and related carbon allotropes, *Carbon*, 2000, **38**, 1529-1534.
24 D. V. Konarev, S. S. Khasanov, A. Otsuka, H. Yamochi, G. Saito and R. N. Lyubovskaya, Magnetic properties and stability of negatively charged doubly bonded C_{120}^{2-} dimers, *New J. Chem.*, 2011, **35**, 1829-1835.
25 S. Lu, T. Jin, E. Kwon, M. Bao and Y. Yamamoto, Highly efficient $Cu(OAc)_2$-catalyzed dimerization of monofunctionalized hydrofullerenes leading to single-bonded [60]fullerene dimers, *Angew. Chem. Int. Ed.*, 2012, **51**, 802-806.
26 Y. Abe, H. Tanaka, Y. Guo, Y. Matsuo and E. Nakamura, Mobility of long-lived fullerene radical in solid state and nonlinear temperature dependence, *J. Am. Chem. Soc.*, 2014, **136**, 3366-3369.
27 L. T. Scott, Fragments of fullerenes: Novel syntheses, structures and reactions, *Pure Appl. Chem.*, 1996, **68**, 291-300.
28 Y.-T. Wu and J. S. Siegel, Aromatic molecular-bowl hydrocarbons: synthetic derivatives, their structures, and physical properties, *Chem. Rev.*, 2006, **106**, 4843–4867.
29 V. M. Tsefrikas and L. T. Scott, Geodesic polyarenes by flash vacuum pyrolysis, *Chem. Rev.*, 2006, **106**, 4868-4884.
30 I. Aprahamian, R. E. Hoffman, T. Sheradsky, D. V. Preda, M. Bancu, L. T. Scott and M. Rabinovitz, A four-step alternating reductive dimerization/bond cleavage of indenocorannulene, *Angew. Chem. Int. Ed.*, 2002, **41**, 1712-1715.
31 I. Aprahamian, D. V. Preda, M. Bancu, A. P. Belanger, T. Sheradsky, L. T. Scott and M. Rabinovitz, Reduction of bowl-shaped hydrocarbons: dianions and tetraanions of annelated corannulenes, *J. Org. Chem.*, 2006, **71**, 290-298.
32 D. Eisenberg and R. Shenhar, Polyarene anions: interplay between theory and experiment, *WIREs: Comput. Mol. Sci.*, 2012, **2**, 525-547.
33 D. Eisenberg, R. Shenhar and M. Rabinovitz, in *Fragments of fullerenes and carbon nanotubes: designed synthesis, unusual reactions, and coordination chemistry*, eds. M. A. Petrukhina and L. T. Scott, Wiley, Hoboken, New Jersey, 2012, pp. 63-93.
34 A. V. Zabula, A. S. Filatov, S. N. Spisak, A. Yu. Rogachev and M. A. Petrukhina, A main group metal sandwich: five lithium cations jammed between two corannulene tetraanion decks, *Science*, 2011, **333**, 1008-1011.
35 A. V. Zabula, S. N. Spisak, A. S. Filatov and M. A. Petrukhina, Self-assembly of charged supramolecular sandwiches formed by corannulene tetraanions and lithium cations, *Organometallics*, 2012, **31**, 5541-5545.
36 A. V. Zabula, S. N. Spisak, A. S. Filatov and M. A. Petrukhina, Pentadecker supramolecules with a lithium alkoxo nanobelt sandwiched between two highly charged buckybowl surfaces, *Angew. Chem. Int. Ed.*, 2012, **51**, 12194-12198.
37 A. S. Filatov, A. V. Zabula, S. N. Spisak, A. Yu. Rogachev and M. A. Petrukhina, Clamshell opening in the mixed-metal supramolecular aggregates formed by four-fold reduced corannulene for maximizing intercalated metal content, *Angew. Chem. Int. Ed.*, 2014, **53**, 140-145.
38 A. S. Filatov, S. N. Spisak, A. V. Zabula, J. McNeely, A. Yu. Rogachev and M. A. Petrukhina, Self-assembly of tetrareduced corannulene with mixed Li-Rb clusters: dynamic transformations, unique structures and record ^{7}Li NMR shifts, *Chem. Sci.*, 2015, **6**, 1959-1966.
39 A. V. Zabula, S. N. Spisak, A. S. Filatov, A. Yu. Rogachev, R. Clérac and M. A. Petrukhina, Supramolecular trap for a transient corannulene trianion, *Chem. Sci.*, 2016, **7**, 1954-1961.
40 S. N. Spisak, A. Yu. Rogachev, A. V. Zabula, A. S. Filatov, R. Clérac and M. A. Petrukhina, Tuning the separation and coupling of corannulene trianion-radicals through sizable alkali metal belts, *Chem. Sci.*, 2017, **8**, 3137-3145.

41 S. N. Spisak, Z. Wei and M. A. Petrukhina, Mixing Li and Cs in the reduction of corannulene for the assembly of a cesium-capped sandwich with a hexanuclear heterometallic core, *Dalton Trans.*, 2017, **46**, 5625-5630.

42 A. Yu. Rogachev, M. Alkan, J. Li, S. Liu, S. N. Spisak, A. S. Filatov and M. A. Petrukhina, Mono-reduced corannulene: to couple and not to couple in one crystal, *Chem. Eur. J.*, 2019, **25**, 14140-14147.

43 S. N. Spisak, A. V. Zabula, M. Alkan, A. S. Filatov, A. Yu. Rogachev and M. A. Petrukhina, Site-directed dimerization of bowl-shaped radical anions to form a *σ*-bonded dibenzocorannulene dimer, *Angew. Chem. Int. Ed.*, 2018, **57**, 6171-6175.

44 L. T. Scott, H. E. Bronstein, D. V. Preda, R. B. M. Ansems, M. S. Bratcher and S. Hagen, Geodesic polyarenes with exposed concave surfaces, *Pure Appl. Chem.*, 1999, **71**, 209-219.

45 B. D. Steinberg, E. A. Jackson, A. S. Filatov, A. Wakamiya, M. A. Petrukhina and L. T. Scott, Aromatic π-systems more curved than C_{60}. The complete family of all indenocorannulenes synthesized by iterative microwave-assisted intramolecular arylations, *J. Am. Chem. Soc.*, 2009, **131**, 10537-10545.

46 A. S. Filatov, L. T. Scott and M. A. Petrukhina, π-π Interactions and solid state packing trends of polycyclic aromatic bowls in the indenocorannulene family: predicting potentially useful bulk properties, *Cryst. Growth Des.*, 2010, **10**, 4607-4621.

47 D. V. Preda, *New chemistry and annulations of corannulene*, Ph.D., Boston College, 2001.

48 M. A. Petrukhina, K. W. Andreini, J. Mack and L. T. Scott, X-ray quality geometries of geodesic polyarenes from theoretical calculations: what levels of theory are reliable?, *J. Org. Chem.*, 2005, **70**, 5713-5716.

49 A. S. Filatov, A. Yu. Rogachev, E. A. Jackson, L. T. Scott and M. A. Petrukhina, Increasing the curvature of a bowl-shaped polyarene by fullerene-like η^2-complexation of a transition metal at the interior of the convex surface, *Organometallics*, 2010, **29**, 1231-1237.

50 S. N. Spisak, A. V. Zabula, A. S. Filatov, A. Yu. Rogachev and M. A. Petrukhina, Selective *endo* and *exo* binding of alkali metals to corannulene, *Angew. Chem. Int. Ed.*, 2011, **50**, 8090-8094.

51 A. V. Zabula, N. J. Sumner, A. S. Filatov, S. N. Spisak, V. M. Grigoryants and M. A. Petrukhina, Reshaping rubrene by controlled reduction with alkali metals, *Eur. J. Inorg. Chem.*, 2012, **2012**, 4675-4683.

52 S. N. Spisak, N. J. Sumner, A. V. Zabula, A. S. Filatov, A. Yu. Rogachev and M. A. Petrukhina, Tuning binding of rubidium ions to planar and curved negatively charged π surfaces, *Organometallics*, 2013, **32**, 3773-3779.

53 A. V. Zabula, Y. V. Sevryugina, S. N. Spisak, L. Kobryn, R. Sygula, A. Sygula and M. A. Petrukhina, An unsolvated buckycatcher and its first dianion, *Chem. Commun.*, 2014, **50**, 2657-2659.

54 S. N. Spisak, J. Li, A. Yu. Rogachev, Z. Wei, O. Papaianina, K. Amsharov, A. V. Rybalchenko, A. A. Goryunkov and M. A. Petrukhina, From corannulene to indacenopicene: effect of carbon framework topology on aromaticity and reduction limits, *Organometallics*, 2016, **35**, 3105-3111.

55 Z. Zhou, S. N. Spisak, Q. Xu, A. Yu. Rogachev, Z. Wei, M. Marcaccio and M. A. Petrukhina, Fusing a planar group to a π-bowl: electronic and molecular structure, aromaticity and solid-state packing of naphthocorannulene and its anions, *Chem. Eur. J.*, 2018, **24**, 3455-3463.

56 C. Bruno, R. Benassi, A. Passalacqua, F. Paolucci, C. Fontanesi, M. Marcaccio, E. A. Jackson and L. T. Scott, Electrochemical and theoretical investigation of corannulene reduction processes, *J. Phys. Chem. B*, 2009, **113**, 1954-1962.

57 M. Alkan and A. Yu. Rogachev, Coupling of two curved polyaromatic radical-anions: stabilization of dimers by counterions, *Phys. Chem. Chem. Phys.*, 2020, **22**, 6716-6726.